Straightening of the Northern San Jacinto Fault, California, as Seen in the Fault-Structure Evolution of the San Jacinto Valley Stepover

Article *in* Bulletin of the Seismological Society of America · December 2011

DOI: 10.1785/0120120232

CITATIONS
17

READS
405

4 authors:

Gayatri Indah Marliyani
Universitas Gadjah Mada
18 PUBLICATIONS **73** CITATIONS
SEE PROFILE

Thomas K. Rockwell
San Diego State University
309 PUBLICATIONS **6,593** CITATIONS
SEE PROFILE

Nate Onderdonk
California State University, Long Beach
20 PUBLICATIONS **149** CITATIONS
SEE PROFILE

Sally Mcgill
California State University, San Bernardino
47 PUBLICATIONS **1,150** CITATIONS
SEE PROFILE

Bulletin of the Seismological Society of America, Vol. 103, No. 3, pp. –, June 2013, doi: 10.1785/0120120232

Straightening of the Northern San Jacinto Fault, California as Seen in the Fault-Structure Evolution of the San Jacinto Valley Stepover

by Gayatri Indah Marliyani,* Thomas K. Rockwell, Nathan W. Onderdonk, and Sally F. McGill

Abstract We investigate a releasing stepover between the Casa Loma and Claremont strands of the northern San Jacinto fault zone to evaluate the Late Quaternary structural evolution of the fault zone, and to assess the likelihood of a rupture jumping across the stepover. Our new cone penetration test (CPT) and trench observations along the Claremont fault at Mystic Lake indicate that the main strand of the Claremont fault has jumped nearly a half kilometer westward into the San Jacinto releasing stepover during the late Quaternary. Multiple faults are inferred from the CPT data within a small sag at the northeast side of the stepover that cuts through younger stratigraphy to the west of the basin-bounding fault near Mystic Lake. Previous seismic-reflection data also suggest the presence of a young fault that cuts basin strata beneath the middle of Mystic Lake farther west of our study area. Numerous tectonogeomorphic features observed in satellite and LiDAR DEM imagery are interpreted to delineate the location of the currently active faults, including a zone of faults that cut across the basin from the northern end of the Casa Loma fault to the Claremont fault. Seismicity observations suggest the presence of many faults within the stepover zone. Finally, new paleoseismic data from the Mystic Lake site suggest that some late Holocene earthquakes may have jumped the stepover. All of these observations suggest that the San Jacinto stepover, which has been used as the primary basis for segmenting the northern San Jacinto fault zone, is being bypassed and that the fault zone may now be capable of larger earthquakes than previously expected.

Introduction

For many historical earthquakes, rupture terminations commonly coincide with major steps, bends, or jogs in a fault, which are then considered or interpreted as segment boundaries (Knuepfer, 1989; Wesnousky, 2006; Sibson, 1986). These geometric discontinuities have been the subject of intensive studies because they are one aspect of fault-zone structure that is easily observable at the surface (Sanders and Magistrale, 1997) and because whether or not a rupture jumps across a stepover influences the ultimate size of the earthquake (Wesnousky, 1994; Oglesby, 2008). The size of a geometrical discontinuity with respect to the rupture length may play an important role in controlling rupture termination, as shown by Wesnousky (2006) in a study of 22 historical earthquakes. In that study, Wesnousky (2006) showed that ruptures jumped across stepover widths of less than 3–4 km about 60% of the time, but did not propagate across larger ones. In this paper we investigate a releasing stepover between the Casa Loma and Claremont strands of the northern San Jacinto fault (SJF) zone to evaluate the Late Quaternary structural evolution of the fault zone and evaluate the likelihood of a rupture jumping across the stepover.

The SJF zone is a major component of the southern San Andreas fault (SAF) system in southern California (Fig. 1). The cumulative movement along this fault has been of oblique type with predominantly right-lateral motion accompanied by a subordinate vertical component (Sharp, 1967). Large earthquakes are known to have occurred along this fault, with at least 10 events of magnitude greater then M_w 6 recorded since 1890. The SJF straightness, continuity throughout its known length, as well as its lateral strain rate, suggest that it may be the most active member in the system of faults in Southern California (Sharp, 1967; Sanders and Kanamori, 1984; Ellsworth, 1990).

The SJF zone consists of several fault strands that are separated by various discontinuities that may act as barriers to lateral rupture propagation, and these have been interpreted as segment boundaries (Sanders and Kanamori, 1984). Seven segments have been identified, with segment lengths ranging from 30 to 90 km (Working Group on California Earthquake Probabilities, 1995, 2007; Field *et al.*, 2009). These include (from north to south) the San Bernardino Valley, Claremont,

*Now at School of Earth and Space Exploration, Arizona State University, ISTB4, Room 795, 781 Terrace Road, Tempe, Arizona 85287-6004.

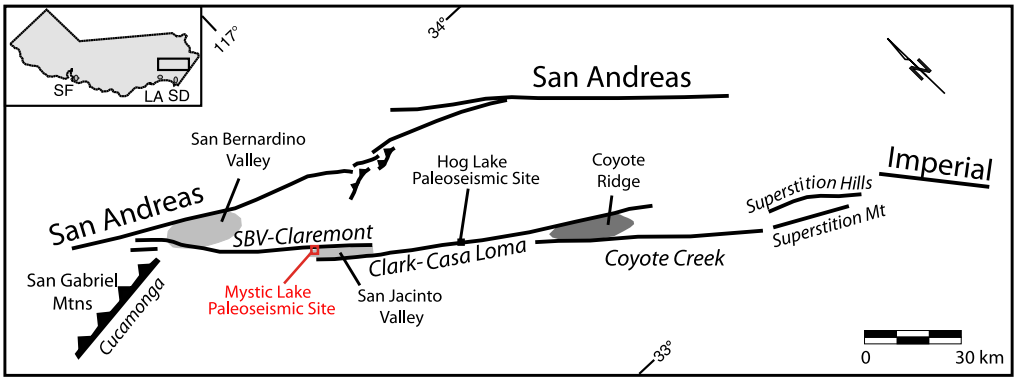

Figure 1. Generalized map of the San Jacinto and southern San Andreas fault zones indicating the large scale segmentation of the fault zones (modified from Sanders and Magistrale, 1997). Location of the paleoseismic sites referenced in the text is annotated as small squares. Inset map shows the state of California as reference. The color version of this figure is available only in the electronic edition.

Casa Loma, Clark, Coyote Creek, Superstition Hills, and Superstition Mountain segments (Fig. 1). At least four significant historic earthquakes are inferred to have occurred along the Clark–Casa Loma fault: the 1899 Christmas Day M_S 6.4 (M_w 7 inferred by Sanders and Kanamori, 1984) and the 1918 M_w 6.9 San Jacinto earthquakes along the northern part of the zone (Rasmussen, 1981; Ellsworth, 1990; Doser, 1992), and the 1937 M_w 5.6 Terwilliger Valley and the 1954 M_w 6.3 Arroyo Salada earthquakes along the central and southern sections of the fault, respectively (Sanders *et al.*, 1986; Doser, 1990). On the northernmost portion of the SJF zone, at least two historical earthquakes were recorded: the July 1899 and the July 1923 earthquakes. The July 1899 M_I 6.5 earthquake (Toppozada *et al.*, 1981) has been suggested by Thatcher *et al.* (1975) to have occurred on the San Bernardino segment of the SJF near Cajon Pass. Meanwhile, the location of the July 1923 M_w 6.4 event is less certain. Sanders and Kanamori (1984) suggest that the earthquake occurred either on the San Bernardino segment of the SJF near Loma Linda or on the San Bernardino Mountain segment of the SAF northeast of the San Bernardino Valley.

Active deformation on the Clark–Casa Loma fault steps right to the Claremont fault to form the releasing San Jacinto Valley stepover (Figs. 1 and 2), which is a linear basin that has been filled by as much as 2.5 km of Quaternary sediments (Christie-Blick and Biddle, 1985; Morton and Matti, 1993). Some workers (Sharp, 1972; Morton and Matti, 2001a, 2001b) have mapped the stepover between the traces of the Claremont and Casa Loma faults segments on the northeast and southwest margins of the basin to be as wide as 4–5 km (Fig. 2a), which according to numerical modeling by Harris and Day (1993) and Harris *et al.* (1991) is large enough to stop rupture propagation. However, other previous studies (e.g., Park *et al.*, 1995; Lee *et al.*, 1996) suggest that the stepover width is considerably less.

We present new interpretations of Light Detection and Ranging Digital Elevation Model (LiDAR DEM) and satellite imagery throughout the basin as well as new results from cone penetration test (CPT) surveys, and analysis of seismicity in the stepover zone. We first describe the current structure of the basin based on our analysis of LiDAR DEMs and satellite imagery. We then provide a brief description of the Mystic Lake site, which is located along the Claremont fault on the northeastern side of the San Jacinto basin, followed by presentation of the new CPT data collected at the Mystic Lake site. We then combine these data with seismicity data and previously published geological and geophysical data (Park *et al.*, 1995; Lee *et al.*, 1996) to interpret the active basin structure of the San Jacinto Valley stepover. We compare our interpretation with paleoseismic data collected from the Mystic Lake site (Onderdonk *et al.*, 2013). Finally, we compare our findings to models of strike-slip-basin formation to provide further insight into the structural evolution of the San Jacinto basin and the current stage of basin development through time.

Methods

We used a combination of field- and remotely based mapping techniques to identify and map active faults in the Mystic Lake site. We also evaluate the CPT and shallow trenches data to further examine which fault strands are currently the most active, and which have mostly ceased their activity.

Surficial Mapping from LiDAR and Air Photos

We examined the San Jacinto Valley stepover using satellite imagery, historic aerial photography, and the high-resolution B4 LiDAR dataset DEMs (Bevis *et al.*, 2005), available through OpenTopography.org to delineate surface features that may be related to faulting. Lineaments that are potentially fault-related were mapped directly on the imagery to produce the map in Figure 2. Some of these lineaments can be identified as scarps, pressure ridges, deflected streams, linear depressions, and sags that are clearly fault-related. Others are of a more questionable origin. Because the local surface gradient parallels the fault in much of this

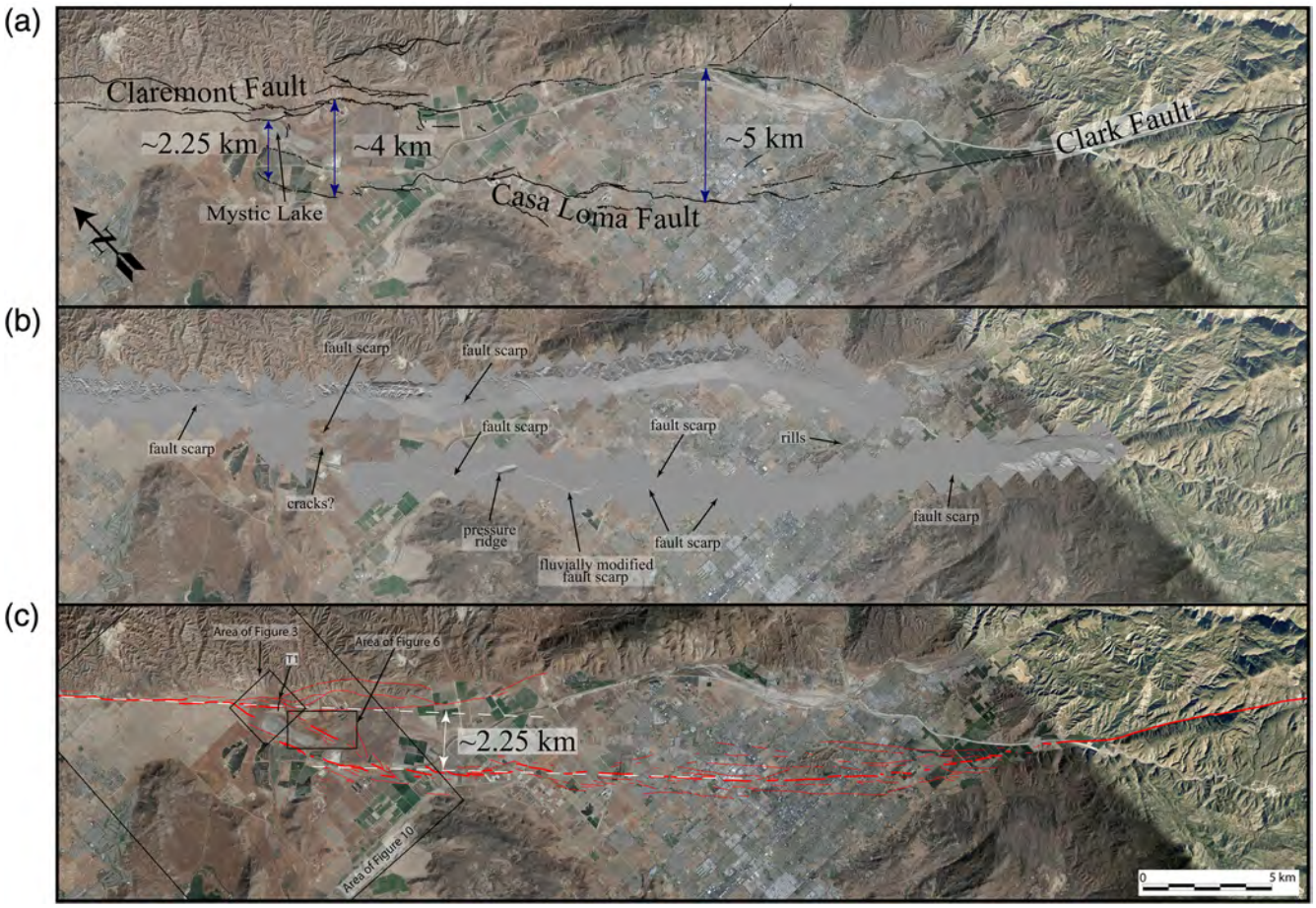

Figure 2. Classical interpretation and reinterpretation of the San Jacinto Valley stepover. (a) The conventionally accepted configuration of the San Jacinto Valley stepover that led to the segmentation model for the Casa Loma and Claremont faults (Working Group on California Earthquake Probabilities, 1995, 2007; Sanders and Magistrale, 1997; Field *et al.*, 2009); the fault lines are adopted from USGS Quaternary fault and fold database; (b) annotated geomorphic features that delineate the active fault strands (scarps, pressure ridges, and lineaments) superposed on LiDAR and Google Earth images; (c) interpretation of the primary active faults within the San Jacinto Valley stepover zone: bold lines, interpreted as the main fault zone; thinner lines, secondary fault strands; dashed lines, lineaments with no obvious vertical or lateral offset. The transfer zone consists of several cross-basin faults that have been identified at the northern end of Casa Loma fault in Mystic Lake. The color version of this figure is available only in the electronic edition.

region, it can be difficult to distinguish fault-controlled rills or channel walls from those that are not fault-related.

Cone Penetrometer Testing Data

CPT data are generated by a truck with internally mounted equipment that inserts a cone-tipped probe downward into the ground. As the probe penetrates, it continuously records the sleeve friction and tip-penetration resistance of the sediments, resulting in a vertical profile of these values that is very sensitive to changes in lithology. CPT surveys can be applied to relatively soft, fine-grained sediments. A group of CPT signatures can be used to identify and correlate sedimentary units between adjacent holes, and these can then be used to create subsurface cross sections and maps (e.g., Grant *et al.*, 1997).

We conducted CPT work along two parallel transects across a small sag feature near the northeastern margin of Mystic Lake and used these data to produce cross sections of the subsurface. The first CPT line (CPT line 1) was located parallel to and just northwest of a 1.5-m-deep locator trench (T1) that was excavated across the sag (Fig. 3). The second CPT transect (CPT line 2) was located approximately 250 m to the southeast of the first transect (Fig. 3). For our study, a total of 38 CPT holes, extending to depths of up to 30 m, were logged along the two transects (Fig. 4).

Faults are recognized in the CPT sections from two or more types of evidence following methods described by Grant *et al.* (1997); by abrupt drop of a vertical sequence of otherwise laterally continuous units, by abrupt changes in unit thicknesses, or by an abrupt change in lithology. Caution was used to differentiate between faulting and facies changes. Upwardly decreasing apparent dips of stratified units were interpreted as a result of faulting whereas dipping units above flat-lying units were interpreted as facies changes. Upward termination of a fault was assumed to be overlain by

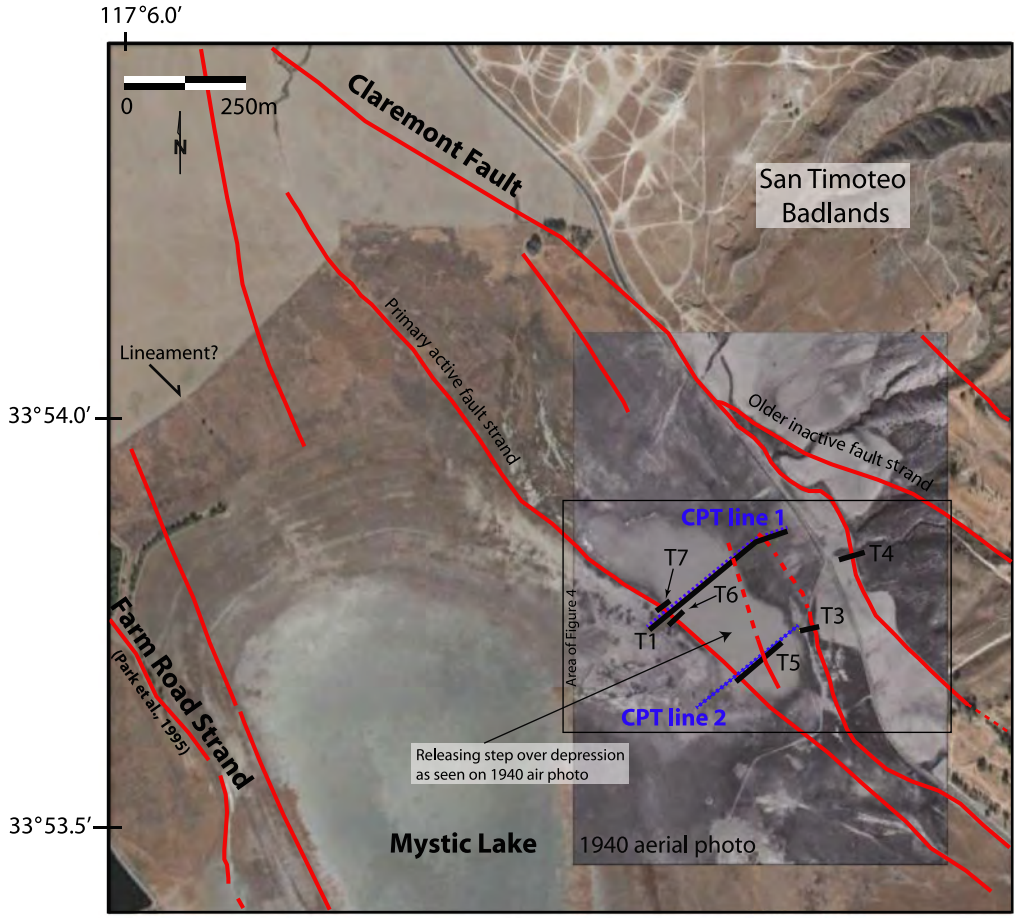

Figure 3. Map of the Mystic Lake site on 1940 aerial photo and Google Earth imagery. Dotted lines marks the CPT transect, heavy solid lines marks the trench location, solid lines represented the interpreted fault lines. The color version of this figure is available only in the electronic edition.

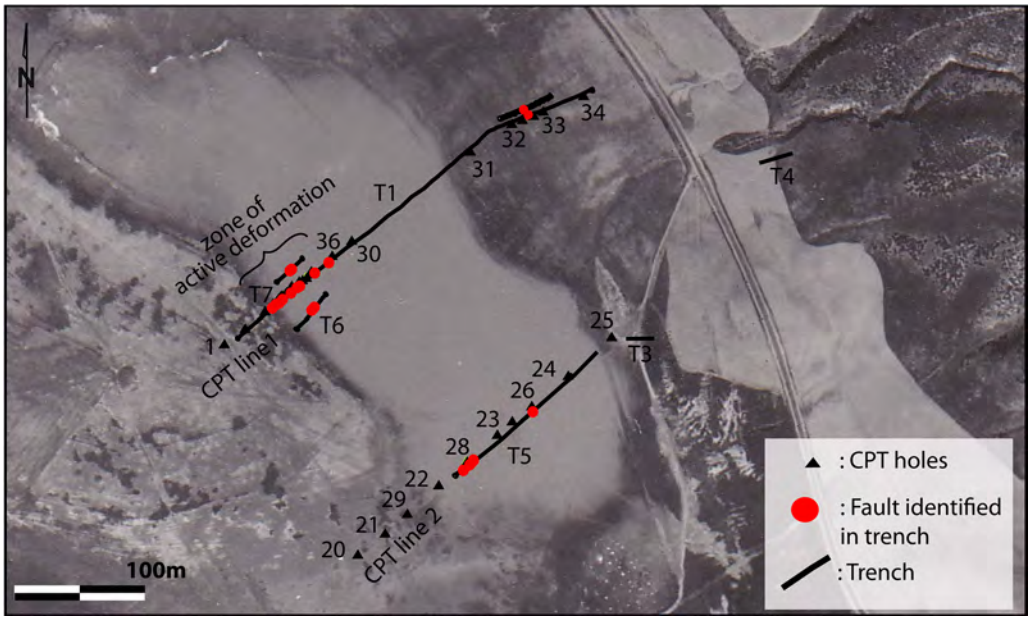

Figure 4. Detailed map of the area of the two CPT lines and trenches. Dots mark the location of each fault strand identified in the trenches. The color version of this figure is available only in the electronic edition.

flat-lying units with uniform thickness. For every suspected fault zone, we constructed plots of depth *versus* apparent vertical displacement. An increasing vertical displacement with depth confirms the fault existence and suggests a history of multiple ruptures.

The fault identification cannot be solely based on stratigraphic changes because some of the features might be caused by a combination of folding and facies changes. In this site, outside of the suspected fault zone, changes in thickness and lithology of most units are gradual from the hillslope to the center of the basin. The thickest units are located closest to the hill-slope and thinning to the center of the basin. Given the lateral continuity of the lithologic units across the site, it is unlikely to interpret that the vertically aligned, abrupt stratigraphic changes were caused solely by depositional processes. Although apparent downdropping of units could indicate either folding or faulting, the accompanying changes in thickness of units are more plausibly the result of displacement and deposition over a scarp (as a result of faulting) than folding.

Stratigraphic correlation shows the thinnest units (unit A, cross section 1) have minimum thicknesses of approximately 25 cm. Therefore, the smallest recognizable vertical offset of the thin-bedded units would be approximately 12 cm. Recognition of faulting in thicker units would require larger vertical offsets.

The locations of the CPT holes were surveyed with a Trimble R8 differential Global Positioning Systems (GPS) system accurate to about ±2 cm vertically and horizontally. This survey provided elevation control for constructing the cross sections.

Shallow Trenches

Along with the collection of CPT data, shallow trenches (mostly 1.5 m in depth) were excavated to identify the near surface, active zone of faulting (Fig. 3). T1 was excavated prior to the CPT survey as a locator trench. T5 was excavated across the main fault zone identified on the second CPT transect. T6 and T7 were excavated after the CPT survey to further examine the main fault zone identified in T1 (see Onderonk *et al.*, 2013). T3 and T4 were excavated across scarps that mark the eastern edge of the sag at the base of the San Timoteo Badlands.

Seismicity Data

To further augment our study, we analyzed the seismicity of the Mystic Lake stepover region for the period from 1980 to 2005, as listed in the LSH.2.1 catalog published by Lin *et al.* (2007). We constructed a map of the distribution of seismicity, along with several cross sections, using MATLAB software. Forty-nine cross sections were constructed perpendicular to the strike of the Claremont and Casa Loma faults at intervals of 0.5 km along the entire length of the San Jacinto basin; some of the most representative cross sections are shown in Figure 5. The cross sections include earthquakes that occurred within 750 m on either side of the 15-km-long projection planes (Fig. 5).

Interpretation of LiDAR Data and Aerial Imagery

Geomorphic interpretation using aerial imagery is a critical element in identifying recently active fault traces (Wallace, 1990). We examined satellite imagery and the high-resolution B-4 LiDAR dataset (Bevis *et al.*, 2005), available through OpenTopography.org, of the San Jacinto Valley stepover to delineate surface features (e.g., lineaments) that may be related to faulting (Fig. 2). We identified several prominent lineaments (vegetation and tonal), pressure ridges, scarps, and differentially incised rills (suggesting old scarps) in the aerial photographs. We field-checked some of these features to confirm that they are related to faulting. Many geomorphic features along the active fault strands in the San Jacinto basin have probably been obliterated by manmade developments and seasonal lake erosion, but many features are still well preserved and observable. This method of imagery interpretation allowed us to document many recently active and significant rupture traces (Fig. 2b,c).

A subsurface fault interpreted by Park *et al.* (1995) and Lee *et al.* (1996) is located below the surface trace of the Casa Loma fault. Prominent left-stepping fault patterns are observed on the western side of the basin where the principal trace of the Casa Loma fault forms several pressure ridges. An obvious scarp observed along the Casa Loma fault on the southwest side of Mystic Lake (labeled as fluvially modified fault scarp on Fig. 2b) is a fluvial modification of a fault scarp that may have originally been located approximately 100 m basinward where more subtle, but younger-looking scarps are also observed. Thus, we interpret these younger scarps as the currently active fault (Fig. 2c). The overall surface trace of the active Casa Loma fault zone exhibits a strike of approximately N55°W in the south and N44°W in the north.

The Claremont fault passes through the northern shoreline of Mystic Lake and comprises three main fault strands in this area (Fig. 3). One of the fault strands cuts through the San Timoteo badlands and is inferred to be older and most likely inactive, based on the fact that it deflects larger streams by 100–120 m, whereas smaller streams that entrench younger Quaternary terraces are not deflected by the fault (Onderdonk *et al.*, 2013). Along the western side of the basin, the northern Casa Loma fault bends toward the Claremont fault. According to our mapping, the present-day step between the Casa Loma and Claremont faults occurs at the northwest end of the San Jacinto Valley. This interpretation is consistent with the presence of Mystic Lake (the lowest point in the basin) at the northwest end of the valley, rather than in the center. Given this location for the step, and our new mapping of the Casa Loma fault, the width of the stepover is only about 2.25 km (Fig. 2c), considering the strike of the Claremont and Casa Loma faults to the northwest and southeast of the step, respectively. In addition, this step is characterized by multiple N25°W-striking faults that create a transfer zone

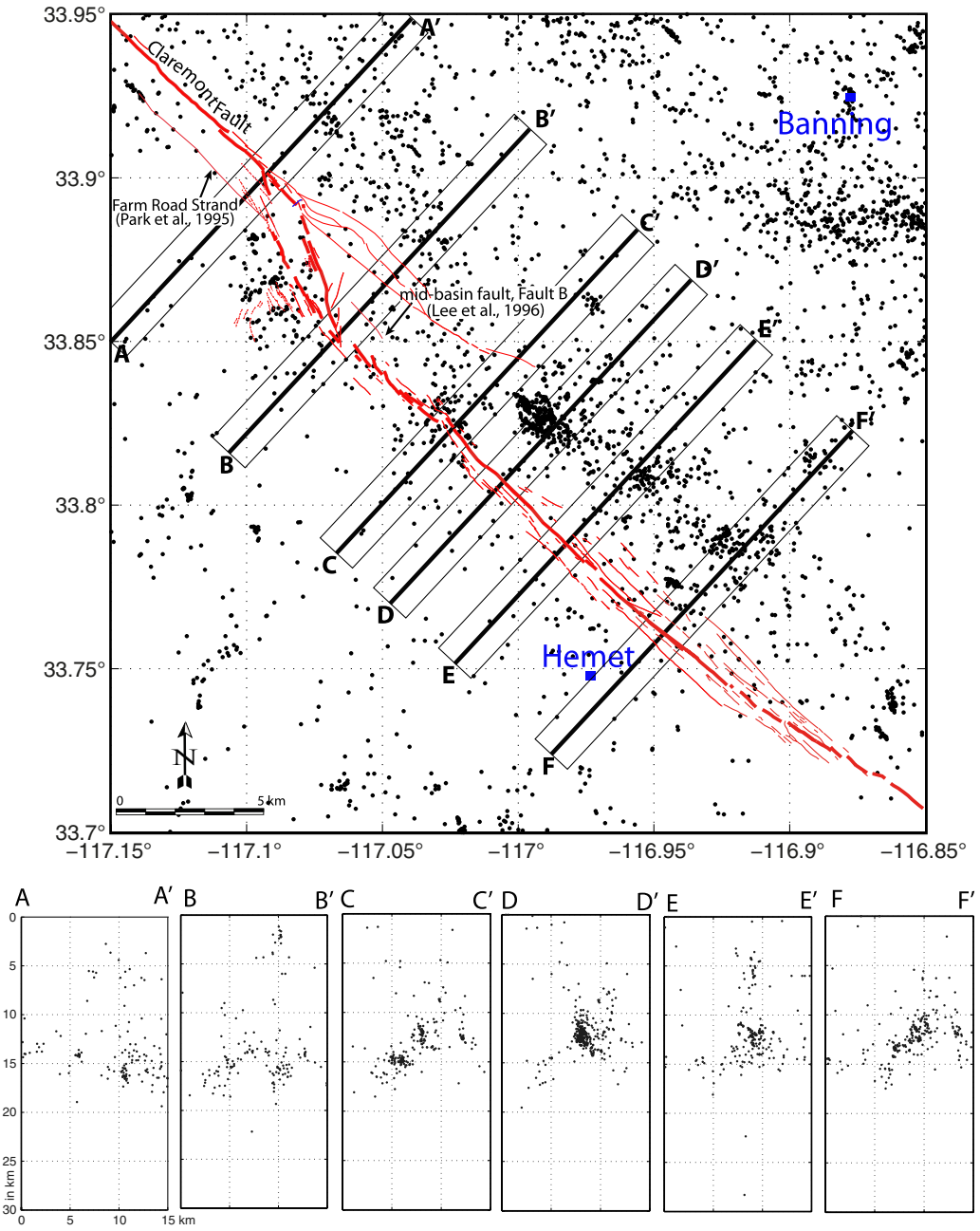

Figure 5. Map of the distribution of seismicity (1981–2005; Lin *et al.*, 2007) within the San Jacinto basin region. Irregular lines represent fault locations as mapped during this study (see Fig. 2c). Depth profiles show earthquakes within 750 m on each side of the profile line collapsed onto the section (see boxes). Depth sections show that much of the seismicity is diffuse and does not readily resolve onto discrete surfaces, suggesting a complex geometry of fault at depth. The color version of this figure is available only in the electronic edition.

from the northern end of the Casa Loma fault to the southern end of the active trace of the Claremont fault (Fig. 6). These cross-basin faults are identified at the surface by the presence of young scarps that would facilitate through-going rupture across the stepover. The 2.25 km width of the stepover is also observable from the U.S. Geological Survey and California Geological Survey (2006; see Data and Resources) Quaternary fault and fold database. Our mapping corroborates this width and adds greater detail on linkage structures between the Casa Loma and Claremont faults.

Subsurface Structure of the Mystic Lake Paleoseismic Site

Mystic Lake is an ephemeral lake that forms in the lowest elevations of the San Jacinto Valley pull-apart basin. It is filled with water during extremely wet winters, so most of our field work was completed during the summer months. Mystic Lake is located at the northwest end of the zone of overlap between the Claremont and Casa Loma faults (Figs. 2 and 3).

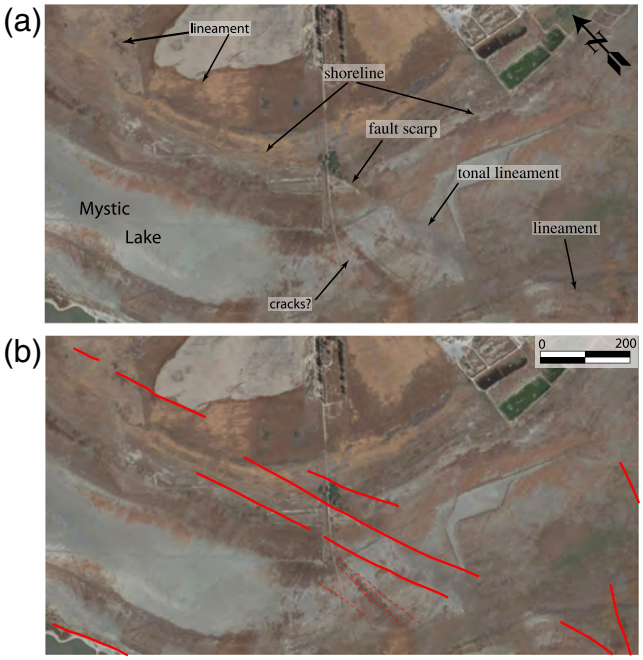

Figure 6. Enlarged images from one part of the transfer zone, northeast of Mystic Lake (location indicated in Fig. 2c). (a) Annotated geomorphic features, including a field-checked fault scarp, that delineate the active fault strands superposed on Google Earth images; (b) our interpretation of the active faults. The color version of this figure is available only in the electronic edition.

A small releasing sag along the Claremont fault was identified in 1940 aerial photographs along the northeastern edge of the larger Mystic Lake (Figs. 3 and 4). We excavated a ~1.5 m deep and 400 m long locator trench (T1) across this sag (along with several shorter trenches) during our first field season at Mystic Lake in 2009 to locate the faults within the sag. In general, the layers are more coarsely grained on the northeastern side of the sag where sand and silty sand dominates and increases in clay content to the southwest. The trench exposed a 50 m wide fault zone near the southwest end. This fault zone consists of numerous faults that offset stratigraphy composed of sand, silt, and clay, with several paleosols (Fig. 7). One minor, recently active fault was recognized near the northeast end of the trench. The stratigraphy was continuous enough to be traced along the full length of T1 which allows documentation of the structure of the basin and correlate faulting events from one fault zone to another.

Two other mapped traces of the Claremont fault were trenched (T3 and T4) and found to cut Early Holocene sediments to produce substantial vertical separation (a few meters), but the amount of lateral slip, if any, as well as the presence of late Holocene activity remain unclear (see Onderdonk *et al.*, 2013).

During the second field season in 2010, we sited our first CPT transect along the northern side of T1 and a second CPT transect approximately 500 m to the southeast. Three additional shallow trenches (T5, T6, and T7) were also excavated (Figs. 3 and 4).

Two cross sections were constructed from the CPT data (Figs. 8 and 9), based on the correlation of distinctive units identified from each CPT hole. The youngest stratum at the top is labeled as unit A in cross section 1 and a in cross section 2, whereas the oldest identified stratum is labeled as unit Y in cross section 1 and unit u in cross section 2. We could not confidently correlate units between the cross sections due to the large distance between CPT line 1 and 2. At least eleven and six faults were recognized in cross sections 1 and 2, respectively.

The shallow trench projection in CPT holes is indicated on Figure 7. At the shallow depth of Trench 1, the CPT data in line 1 correspond closely with trench observations to within 10 cm resolution (Fig. 10). Specifically, unit J of the CPT transect correlates to unit 800 (radiocarbon age: ~1700 rcy B.P.) identified at the bottom of Trench 1 at a depth of 1.4 m (Fig. 10). This correlation is based on both depth and lithology. Based on the CPT correlations, unit J reaches a maximum depth of ~9 m on the downthrown side of the fault zone, yielding a late Holocene sedimentation rate of more than 5 mm/yr in the sag. This rate is similar to the 3–5.6 mm/yr sedimentation rate estimated for the San Jacinto basin (Morton, 1977). If this rate is representative of the entire sampled section, the oldest units penetrated by our CPT line are probably Early Holocene in age, on the order of 7000 years.

The CPT correlations, along with direct observations from the shallow trench exposure, demonstrate that the main, currently active strand of the Claremont fault comprises a zone of faulting that is tens of meters in width (Figs. 4 and 8). Most major faults identified at depth in the CPT lines were also observed in the trenches, with the interpreted main fault in Trench 1 being the same as Fault 1E in CPT profile 1 (Fig. 8). Away from the main zone of faulting, there are two faults located between CPT 32 and 33 (faults 1A and 1B; Fig. 8). These faults are located approximately 100 m to the west of the older, inactive strand of the Claremont fault identified in T3, and 300 m east of the currently active main trace identified in T1 (Fig. 4). Fault 1A is apparently inactive as it appears to only offset units M and deeper (Fig. 8), and a fault was not observed at this location in Trench 1; Fault 1B likely corresponds to a fault we observed in Trench 1, between holes CPT 34 and CPT 38.

We estimated the vertical separation of every distinctive layer across each fault in the CPT profiles, as illustrated in Figures 8 and 9. The measurements confirm the general trend of increasing displacement with depth for the main fault zone, an observation that is consistent with multiple rupture events. However, some faults to the west of the main fault (e.g., faults 1F and 1I) have similar separation at depth from unit M (about 10 m) downward, which suggests that they initiated motion in the middle Holocene (about 4 ka, if the sedimentation rate has been constant), and are therefore younger than faults to the east. Thus, the CPT observations

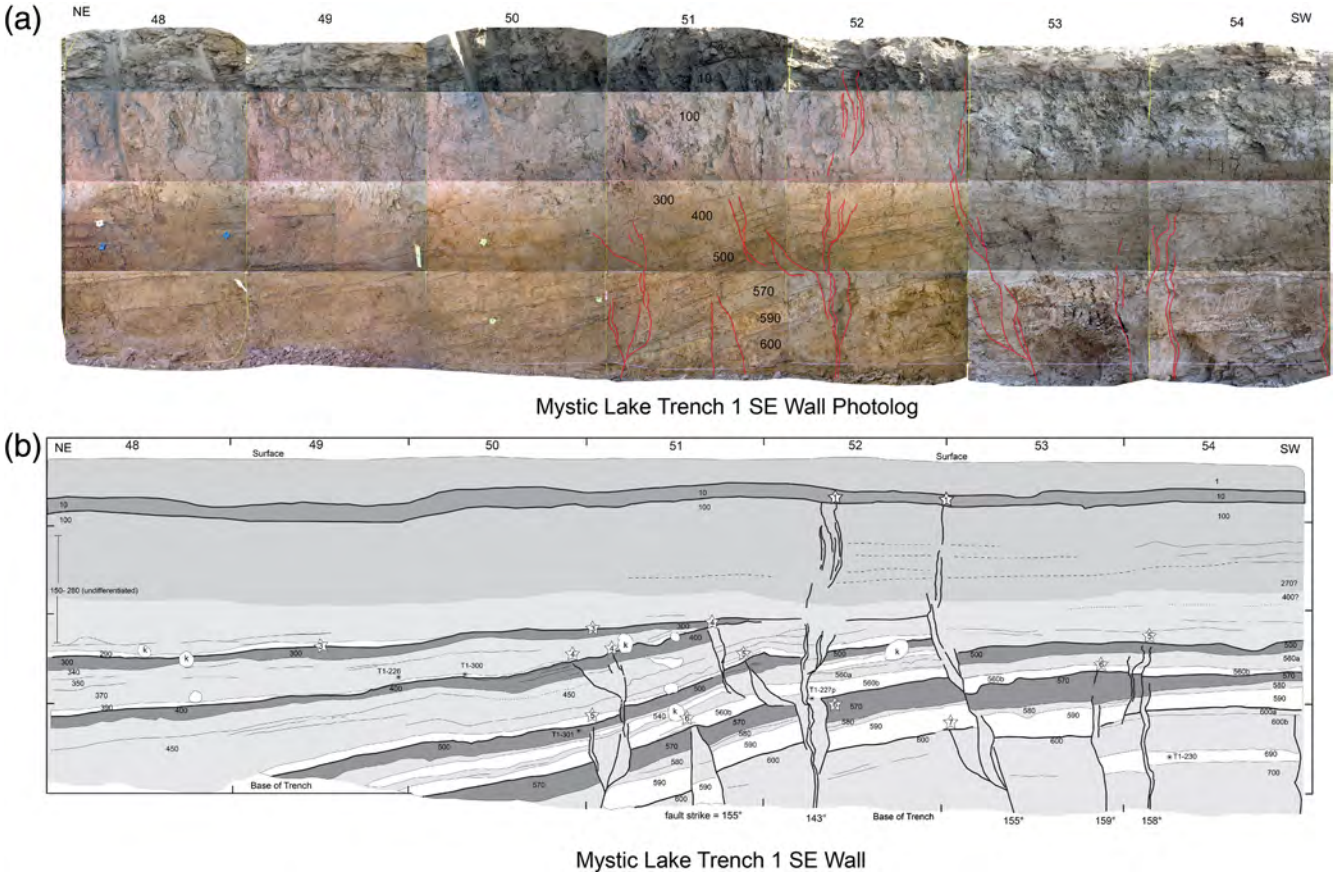

Figure 7. (a) Photomosaic of the main fault zone on the southeast wall of Trench 1. Grid lines are spaced 1 m horizontally and 0.5 m vertically. Faults are traced for clarity. (b) Interpretation redrawn from photologs. Events horizons are marked as bold lines, lines with star denoting event number. Darker gray shades indicate paleosol layers and lighter shades indicate distinct clay layers that typically overlie event horizons (modified from Onderdonk *et al.*, 2013). The color version of this figure is available only in the electronic edition.

suggest that the faults along the northeast side of Mystic Lake may decrease in age towards the center of the basin, which would suggest that the width of the stepover is decreasing. The older trace of the Claremont fault, which has sustained only minor Holocene lateral slip based on the geomorphology and trench evidence (T3 and T4; Onderdonk *et al.*, 2013), is nearly 0.5 km to the northeast of the currently main strand (Fig. 3). These observations all indicate that the primary activity of the Claremont fault has jumped towards the basin in the late Quaternary.

Seismicity Observations

We found it difficult to correlate the surficial faults with the subsurface alignments of microseismicity in this area. Although some vertical cross sections show that the seismicity delineates a near-vertical plane that extends to depths of 10–15 km (cross section E, Fig. 5), in most places the distribution is fairly broad and diffuse (Fig. 5). In some places there is better correlation between active surface structure and seismicity at depth, such as in cross section CC′, where several fault strands at the surface coincide with the surface-projection of several steeply dipping faults at around 10–15 km depth. A cluster of seismicity appears to occur southeast of the southern tip of the trace of Claremont fault. However at depth, as observed from profile DD′ (Fig. 5), we cannot confidently determine the dip of the fault nor unambiguously correlate the seismicity with surface faults. Although it appears that there is a very weak northeast-dipping alignment of seismicity that may project to the surface at the Casa Loma fault (Fig. 5, cross section DD′), there is also an indication that the seismic activity is occurring at depth along the Claremont fault. Areas along the fault zone with few earthquakes, such as the area between cross sections D and E, might suggest that the faults here are seismically locked or inactive, although a longer term of observation is needed to prove it.

Discussion

The field- and remotely-based mapping, CPT, and shallow trench data all indicate that the active deformation at the San Jacinto basin is now closer to the center of the basin. The data also show that the mapped fault traces at the southeast-extension of the Claremont fault are currently inactive and the primary activity of the Claremont fault has jumped

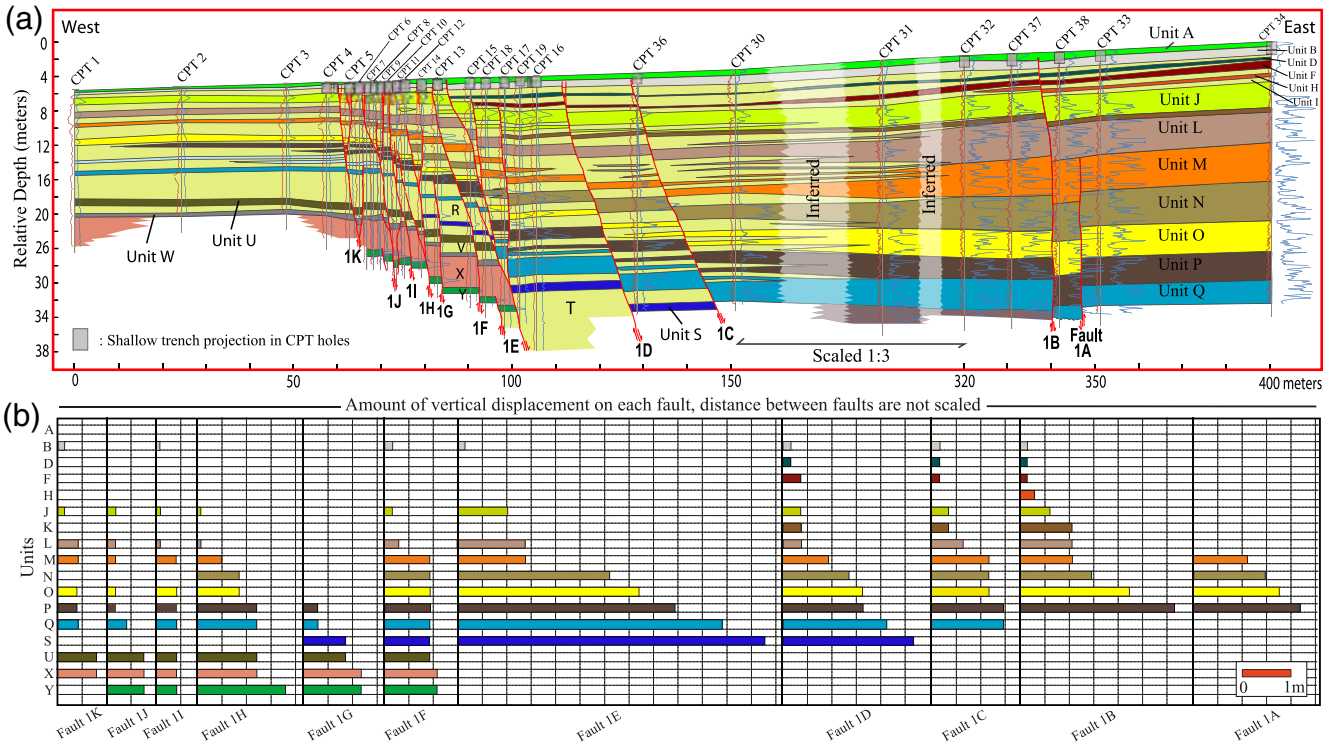

Figure 8. (a) Cross section 1 constructed from compilation of CPT data along transect 1. Note that the vertical scale is exaggerated (vertical exaggeration, 1.8), and the horizontal scale is compressed in the middle of the transect. (b) The measured values of vertical separation of each distinctive unit across each of the identified faults. The color version of this figure is available only in the electronic edition.

towards the basin by ~0.5 km. We compare our data with seismicity, published subsurface and regional paleoseismic data, and physical model of a pull-apart basin. We further assess the implication of the current structure configuration to the rupture pattern along the SJF.

Comparison of Surface Mapping with Seismicity

The seismicity data poorly correspond with the mapped active traces at the surface (see Fig. 5, cross section DD′). Disassociation between mapped surface traces of the fault and the seismicity could be indicative of complex geometry at depth. We interpret down-dip fault segmentation as possible explanation for complexity of seismicity at depth as described by Nemser and Cowan (2009). Nemser and Cowan (2009), based on analyses of cross sections of seismicity at the southern SJF zone, reveal that the down-dip termination of clusters of shallow earthquakes tends to roughly coincide with the up-dip termination of deeper earthquakes. This may indicate down-dip fault segmentation, which is also evident in outcrop-scale observations of the southern SJF zone.

In the San Jacinto Valley stepover area, the microseismicity is fairly diffuse. We interpret the diffuse microseismicity distribution as evidence that the Claremont–Casa Loma fault stepover comprises a complex broad band of right-lateral shear, rather than a single fault at depth.

Although diffuse microseismicity can be due to error in earthquake location, the seismicity used here has been relocated (Lin *et al.*, 2007), so its diffusivity is more likely reflecting the presence of many faults within the stepover zone. This is consistent with field observation, and with the hypothesis that new intrabasin faults have formed that are accommodating the straightening of the northern SJF. However, the relocated catalog of Lin *et al.* (2007) only includes a few decades of data, making it inadequate for rigorous interpretation.

Comparison of Surface Mapping with Published Subsurface Data in the Basin

Park *et al.* (1995) proposed that the San Jacinto Valley pull-apart basin is not a simple rhombochasm, based on its unusual width–length ratio and on geophysical studies that suggest a more complex structure. During their study, three high-resolution shallow seismic-reflection lines were acquired in the northern part of the San Jacinto graben revealing structures in the upper (500–1000 m) part of the basin. The deeper structures were mapped using gravity data. They identified at least one major intragraben structure, which they named the Farm Road Strand (Figs. 3 and 5). This fault is inferred to run parallel to and lie in between the Casa Loma and Claremont strands, and it approximately coincides with an alignment of relocated earthquakes of Sanders and Magistrale (1997).

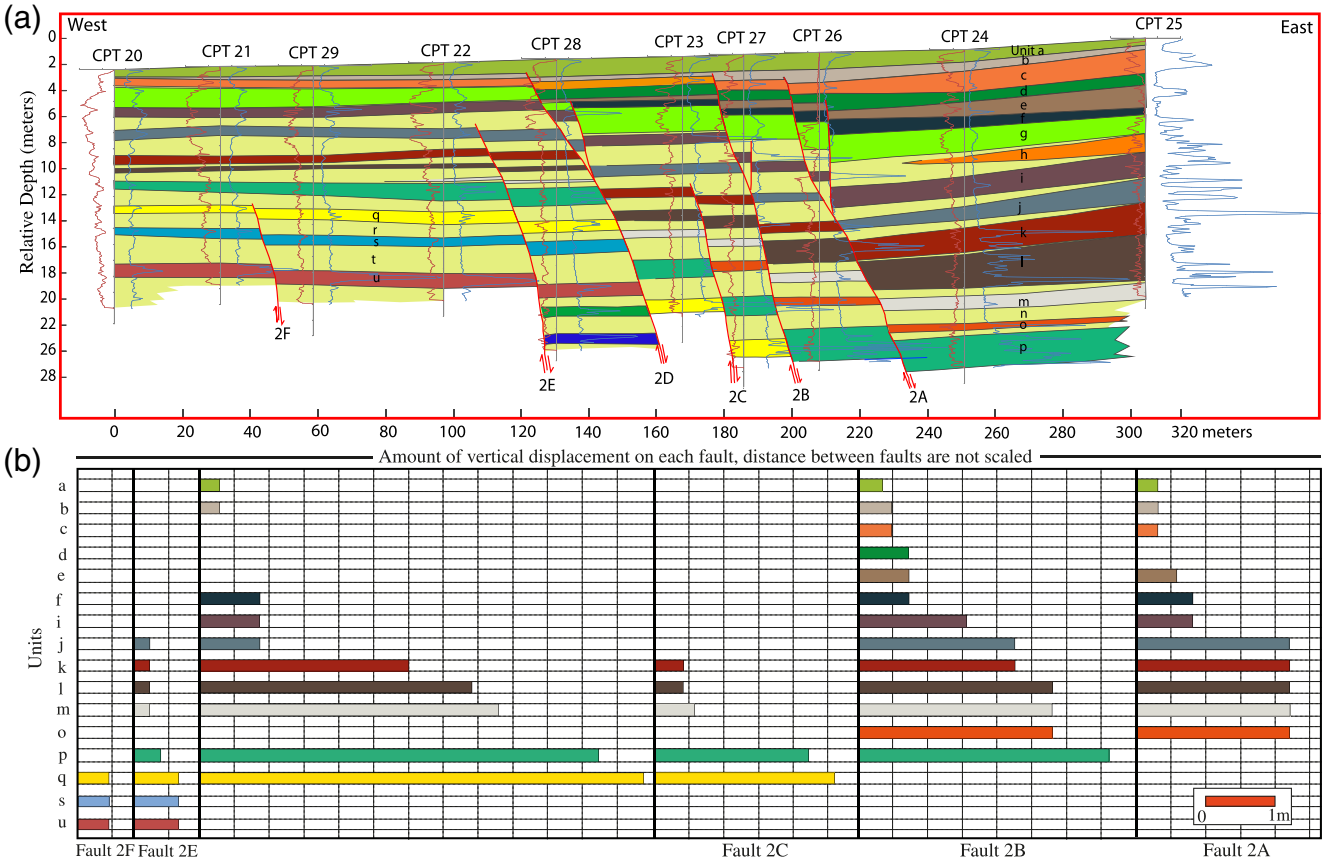

Figure 9. (a) Cross section 2 constructed from correlation of distinctive units identified from each CPT log along CPT transect 2. As with cross section 1, the vertical scale is exaggerated (vertical exaggeration, 3.8). (b) Measured values of vertical separation of each distinctive unit across each of the identified faults in transect 2. The color version of this figure is available only in the electronic edition.

The gravity model constructed by Park *et al.* (1995) shows that the Farm Road Strand, rather than the Casa Loma strand, is the western boundary of the deepest part of the sedimentary basin in the northern San Jacinto Valley (Fig. 11). The basement forms a median step block bounding the San Jacinto graben between the Casa Loma fault to the west and the Farm Road fault. In the mid-basin area, the basement is shallow (400–800 m) to the west of the Farm Road fault and steps down steeply to a depth of 2.5 km to the east of the Farm Road fault.

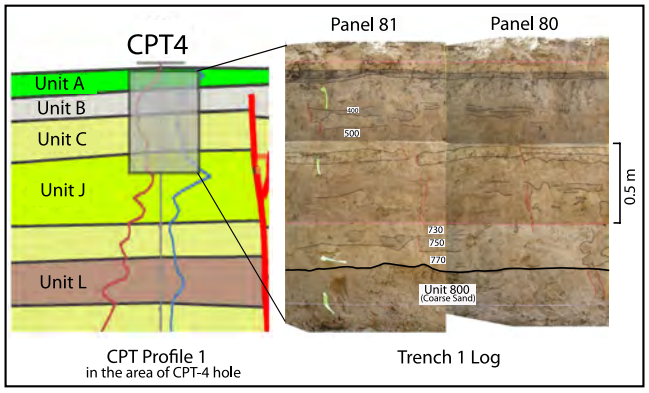

Figure 10. Enlargement of portions of CPT transect 1 (near the CPT-4 hole) and Trench 1 showing that unit J on CPT transect 1 correlates to unit 800 identified at the bottom of Trench 1, at a depth of 1.4 m. The color version of this figure is available only in the electronic edition.

These observations led Park *et al.* (1995) to conclude that the San Jacinto graben is better represented as several offset depocenters bounded by stepping faults, rather than as a single basin with an unusually long overlap ratio. In their model, the series of smaller basins are best represented with average length–width ratios (4:3). According to some previous models of pull-apart-basin evolution (Aydin and Nur, 1982; Mann *et al.*, 1983; Hempton and Neher, 1986), this pattern of offset sedimentary basins resembles the model of coalescing en echelon basins (Fig. 12).

Seismic refraction and reflection studies by Lee *et al.* (1996) in the central San Jacinto basin have identified at least three faults within the basin in addition to the Casa Loma and Claremont faults. One of the fault zones, Fault B (Fig. 5), consists of several minor faults that occur only in the older stratigraphy; they are spaced about 40–80 m apart and have no observed surface expression. Thus, these faults have never been reported in the literature prior to the work of Lee *et al.* (1996). A second fault zone was named Fault D and lies near the presently mapped trace of the Casa Loma Fault. A third

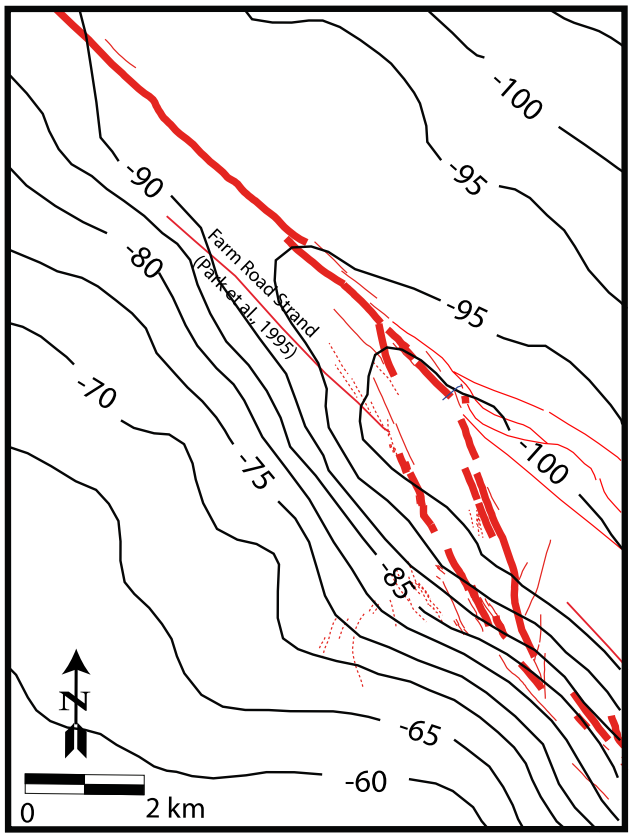

Figure 11. Bouguer gravity anomaly contour map of the northern part of the San Jacinto basin (after Park *et al.*, 1995) with the faults identified during this study superposed on the gravity data. Note that the faults we identified from surface scarps crosscut the deep basin interpreted from the gravity data, suggesting that the deep basin is no longer the main depocenter. Location of the map is shown in Figure 2c. Lines with number attached, Bouguer gravity contour lines; lines with no number attached, fault lines; refer to Figure 2 caption for fault symbology. The color version of this figure is available only in the electronic edition.

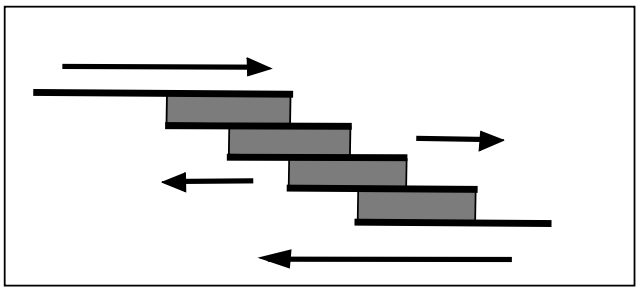

Figure 12. Scale independent model of a pull-apart basin created by coalescing of rhombohedral grabens associated with en echelon dextral strike-slip faults (Aydin and Nur, 1982; cited in Park *et al.*, 1995).

fault, Fault E, is located at the southern end of their seismic lines, but according to Lee *et al.* (1996), its presence is not certain because the reflector disruptions are possibly due to interferences of basement relief, passing traffic, or activity associated with a local store that may have affected data quality.

The Farm Road fault is approximately 1 km from the Casa Loma strand and 2 km from the Claremont strand (Fig. 11) and was considered by Park *et al.* (1995) to be the currently active basin-bounding fault on the west side of the basin. However, based on the presence of scarps (Fig. 2b), we interpret the currently most active strands to be within the basin itself, crosscutting the earlier faults, which may include the northernmost Casa Loma and Farm Road faults. From our CPT study at Mystic Lake, the main currently active fault on the northeast side of the basin is Fault 1E (Fig. 8), which coincides with the main fault observed in Trench 1 and is located 0.5 km to the west of the older strand of the Claremont fault that marks the front of the Timoteo Badlands (Fig. 3). These observations and interpretations all suggest that the width of the fault step in this area is only a couple of kilometers and that there are cross-basin linkage-structures that have evolved to transfer slip. We must note though that the fault arrangement indicated with bold lines in Figure 2c is an interpretation of the main fault structure and does not include all the active-appearing faults in the area.

Comparison of Shallow Trenches with Regional Paleoseismic Data

Recent paleoseismic work at Mystic Lake has documented evidence of seven events over the past 1600 years in the uppermost 2.5 m of the section. The paleoseismological aspect of the site was described in detail in Onderdonk *et al.* (2013). We compared the paleoseismic record from Mystic Lake with ruptures documented at the Hog Lake paleoseismic site, which is located 50 km to the south along the central SJF. These two sites are separated by the San Jacinto Valley stepover, so if the documented ruptures on both faults are similar in ages, this may indicate that some of the large earthquakes have jumped across the stepover.

The age ranges for four of the past seven most recent events at Mystic Lake (Onderdonk *et al.*, 2013) overlap in time with the possible ages of ruptures documented at the Hog Lake paleoseismic site (Rockwell *et al.*, 2000, 2006). This observation suggests that some large San Jacinto events may jump across the San Jacinto Valley releasing stepover, or that stress triggering along one segment causes the other to fail in close succession (Onderdonk *et al.*, 2013).

The strand of the Claremont fault that marks the front of the badlands and exhibits the most dramatic scarps has sustained only minor Holocene strike-slip activity, based on trench evidence (T3 and T4; Onderdonk *et al.*, 2013), and is nearly 0.5 km to the northeast of the main strand identified in trenches and CPT lines. These observations all indicate that the primary activity of the Claremont fault has jumped towards the basin by this amount in the late Quaternary.

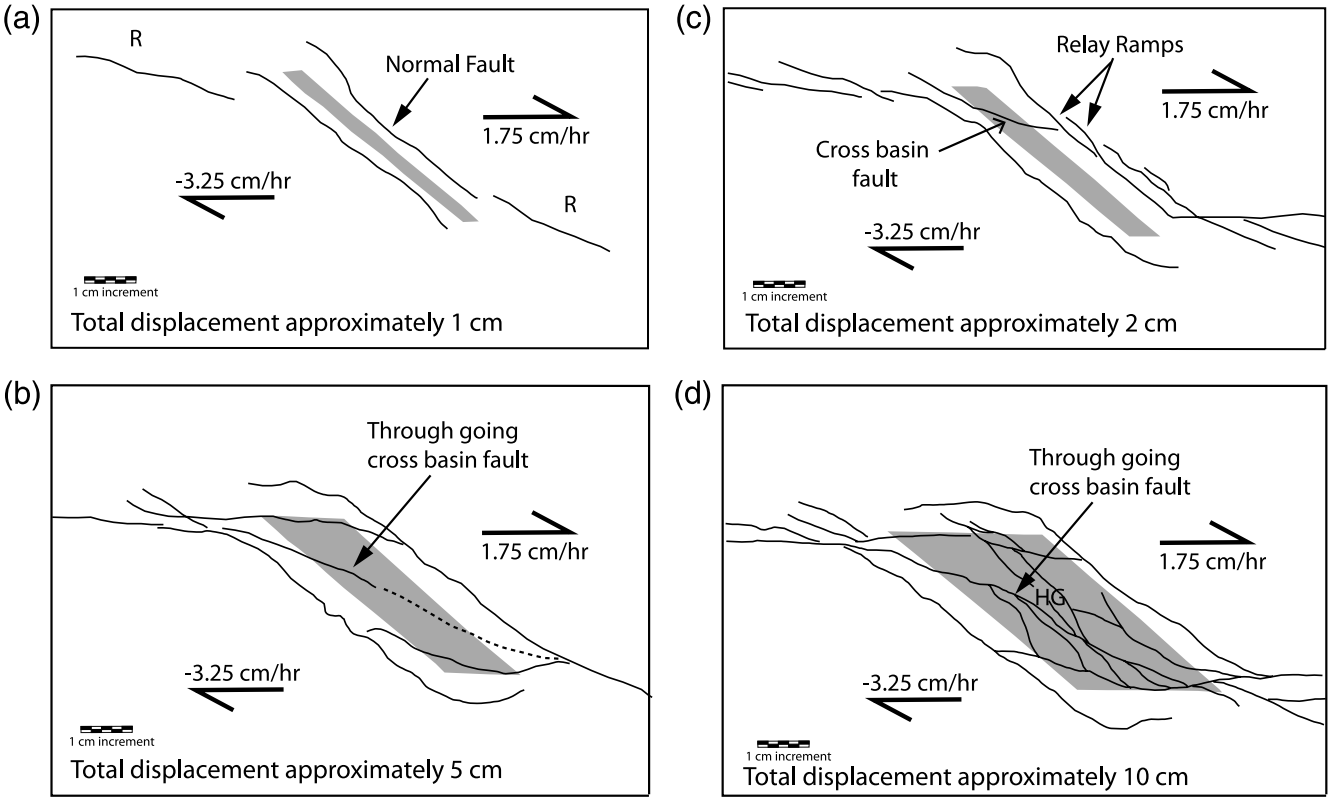

Figure 13. Line drawings illustrating development of a pull-apart basin in a sand-analog model developed by Rahe *et al.* (1998). (a) Formation of normal faults bounding the pull-apart basin during the incipient stage of basin development, (b) development of relay ramps and a cross-basin fault, (c) through-going cross-basin fault early in the mature stage of development, and (d) fully mature pull-apart basin with complex array of normal, strike-slip, and oblique faults; gray shading, zone of subsidence. Note the presence of through-going cross-basin faults that define the mature stage of basin development, similar to what we observe for the San Jacinto basin.

Comparison to Models of the Evolution of Extensional Jogs and Pull-Apart Basins and Slip-Transfer Mechanisms

Physical (e.g., sandbox or clay) models of pull-apart basins can provide insights into strike-slip basin evolution by simplifying their geometry and rheology (e.g., Chinnery, 1966; Tchalenko, 1970; Rodgers, 1980; Segall and Pollard, 1980; Naylor *et al.*, 1986; Zachariasen and Sieh, 1995; Rahe *et al.*, 1998).

In their sand analog model, Rahe *et al.* (1998) used unequal motion on crustal blocks on opposite sides of a strike-slip fault using dry sand above a horizontal detachment horizon. They described the structural evolution of a pull-apart basin in terms of incipient, early, and mature developmental stages (Fig. 13). The incipient pull-apart basin begins by formation of steeply dipping normal faults approximately parallel to the step-angle (in their model set as 40°) of the pure strike-slip section of the horizontal detachment horizon (Fig. 13a). This is followed by the development of Riedel shears above the strike-slip regions (labeled as R in Fig. 13a). Widening across the pull-apart basin is accommodated by formation of additional normal faults parallel to the outer boundary faults of the actively forming graben or half-graben. The incipient stage of pull-apart basin development ends as cross-basin strike-slip faults form diagonally across the pull-apart basin (Fig. 13b). Progressive strike-slip eventually leads to the development of cross-basin faults that shift deformation toward the center of the basin and result in the linkage of strike-slip-fault segments to produce a through-going fault (Fig. 13c). Finally, the mature stage of pull-apart basin development is defined by the presence of a through-going strike-slip fault, created by the coalescing of appropriately oriented earlier-formed segments of the system (Fig. 13d).

The models presented by Rahe *et al.* (1998; Fig. 13d), with their resulting deformation, most closely resemble the configuration of the San Jacinto basin that we interpret from the combination of geomorphic, trench, and CPT observations. The presence of a transfer zone consisting of several cross-basin faults at the northern end of the Casa Loma fault, as identified from the LiDAR DEMs and aerial imagery, indicates that the basin is in such a mature stage of development as modeled by Rahe *et al.* (1998). Strong similarities with the San Jacinto basin include the presence of cross-basin faults, and a mid-basin ridge (HG structure in the physical model, Fig. 13d), indicated by water ponding against the scarp of the main fault in T1 as observed in the 1940 aerial photographs (Fig. 3). As shown in the sandbox-analog models, during the final stage of pull-apart basin development,

displacement on the normal bounding faults slows or stops. As a result, the cross-basin faults in the interior of the pull-apart basin experience increasing rates and larger amounts of normal slip. The faults merge and coalesce, and cross-basin faults transect the full length of the pull-apart basin, linking the two main regions of strike-slip displacement (Figs. 2c, 3, and 13d). The linkage of the main strike-slip displacement zones in the mature stage would dramatically increase the overall area of slippage in a single earthquake and thus the potential for larger magnitude earthquakes.

The cross-basin faults could transfer slip through the San Jacinto Valley stepover during large earthquakes, although slip transfer across a stepover is not required for a step width of only ~2 km (as modeled by Harris and Day, 1993 and Harris *et al.*, 1991).

Implications for Rupture Patterns along the SJF

Based on our interpretation of the current configuration of the main structural elements of the SJF zone in the vicinity of the San Jacinto Valley stepover, it appears that the stepover width is now about 2.25 km. This is considerably less than the 4–5 km proposed by Sanders and Magistrale (1997), who suggested that the stepover is large enough to stop large earthquake ruptures; this was the primary basis for segmenting the northern SJF into the Casa Loma and Claremont faults (Sharp, 1967, 1972, 1975; Matti *et al.*, 1985, 1992; Wesnousky, 1986; Sanders and Magistrale, 1997).

Farther south along the SJF, geological mapping by Sharp (1967) characterized the Casa Loma and Clark faults as separate segments. Other worker have considered these two fault elements as one continuous segment (Wesnousky, 1986), as the two strands are essentially collinear. Moreover, the presence of scarps in the LiDAR DEMs that delineate a continuous zone of faulting support the interpretation that these are essentially a single fault zone. Further, recent observations of slip in the most recent large earthquakes on the Clark fault (Salisbury *et al.*, 2012) also indicate that it is likely that Clark fault ruptures may have extended considerably farther north than Hemet onto the Casa Loma fault. Substantial slip is documented for each of the past several large earthquake ruptures on the south side of Hemet where the fault passes into deep alluvium out of Blackburn Canyon (with the exception of the inferred 1918 rupture, which was a relatively small event; Salisbury *et al.*, 2012).

From the above discussion, it appears plausible that rupture of the entire Clark–Casa Loma–Claremont fault zone, a distance of nearly 200 km, could potentially occur and result in an earthquake as large as M_w 7.6, rivaling the size of expected earthquakes on the SAF. If such an earthquake were to occur, it would be sufficiently large to cause very strong shaking, and potentially substantial damage to the Riverside and San Bernardino areas in southern California. Furthermore, long ruptures may generate a substantial component of their energy in the long-period spectrum, which may excite the deep basins of southern California, including the densely populated areas of Los Angeles and Orange counties. Expected effects would include significant primary surface faulting along the trace of the Clark–Casa Loma–Claremont fault, landslides within the Santa Rosa, San Jacinto, and San Bernardino Mountain areas and other areas with steep terrain, and possibly lateral spreading induced by liquefaction in basins and river valleys where susceptible conditions predominate.

Conclusions

We have presented new geological CPT data that show that the primary active faults of the Mystic Lake stepover on the northeastern side of the San Jacinto basin lie within Mystic Lake itself, with the currently active fault located nearly 0.5 km to the west of the older strand of the Claremont fault that marks the front of the Timoteo Badlands. The CPT observations also suggest that the faults within Mystic Lake are apparently more active and are possibly younger towards the center of the basin. The 1E fault, which accommodated the most dip-slip separation, is currently the primary strand of the Claremont fault. Its large vertical offset and its continuity indicate that it is probably the most mature of the observed intrabasin faults. By contrast, the eastern splays (fault 1A and 1B), although we have no quantitative measure of their age, appear significantly less developed and fault 1A appears to be inactive.

We have also presented new mapping of the location of the currently active faults along the Clark–Casa Loma trend, and within Mystic Lake itself, from the interpretation of satellite imagery and LiDAR DEMs. We identify a transfer zone from the northern end of the Casa Loma fault to the southern end of the active trace of the Claremont fault that appears to crosscut the inferred location of the Farm Road fault. This zone is characterized by multiple N25°W-striking strands interpreted from the presence of scarps and other lineaments; these appear to be the dominant faults in the late Quaternary to have accommodated slip across the basin. Collectively, these new observations, combined with previous work, all argue that the San Jacinto basin stepover has evolved towards a straighter trace and may now be small enough to allow ruptures to pass through, thereby dramatically increasing the plausible size of earthquakes on the SJF.

Data and Resources

The B4 LiDAR dataset DEMs used in this research was acquired in May 2005 as a pre-earthquake survey of the SAF and SJF zones in southern California. For more information about the B4 project, please visit http://www.earthsciences.osu.edu/b4/Site/Welcome.html (last accessed January 2013). The B4 LiDAR dataset is available in many formats via http://www.opentopography.org (last accessed January 2013) for neotectonic and paleoseismic research. The Quaternary fault and fold database was obtained from the U.S. Geological Survey and California Geological Survey

accessed through http://earthquake.usgs.gov/hazards/qfaults/ (last accessed February 2013). The MATLAB software was used to construct the seismicity distribution map and cross section.

Acknowledgments

We would like to thank a number of San Diego State University (SDSU), California State University of San Bernardino (CSUSB) and California State University (CSU) students, Southern California Earthquake Center (SCEC) interns, and visiting researchers that assisted with fieldwork during this study and made this possible. These include Rebecca Tsang, Nissa Morton, Barrett Salisbury, Mike Buga, Katie Farrington, Eulalia Masana, Neta Wechsler, Hurien Helmi, Mark Swift, Brian Anderson, Karina Chung, John Duncan, Ramon Hancock, Scott Kenyon, and Blaise Delgado. We thank Shuo Ma for discussion on the seismicity data analysis. We also thank Eliza Nemser, Ivan Wong, and an anonymous reviewer for their excellent and thorough reviews. This research was supported by funding from the SCEC and a National Science Foundation (NSF) Grant (G00008274). SCEC is funded by NSF Cooperative Agreement EAR-0106924 and U.S. Geological Survey (USGS) Cooperative Agreement 02HQAG0008. The SCEC Contribution Number for this paper is 1628.

References

Aydin, A., and A. Nur (1982). Evolution of pull-apart basins and their scale independence, *Tectonics* **1,** 91–105.

Bevis, M., K. Hudnut, R. Sanchez, C. Toth, D. Grejner-Brzezinska, E. Kendrick, D. Caccamise, D. Raleigh, H. Zhou, S. Shan, W. Shindle, A. Yong, J. Harvey, A. Borsa, F. Ayoub, R. Shrestha, B. Carter, M. Sartori, D. Phillips, and F. Coloma (2005). The B4 Project: Scanning the San Andreas and San Jacinto fault zones (abstract H34B-01), *Abstr. Programs AGU*, H34B-01.

Chinnery, M. A. (1966). Secondary faulting, *Can. J. Earth Sci.* **3,** 163–190.

Christie-Blick, N., and K. Biddle (1985). Deformation and basin formation along strike-slip faults, in *Strike-Slip Deformation, Basin Formation, and Sedimentation*, N. Christie-Blick and K. Biddle (Editors), Vol. 37, Special Publication—Society of Economic Paleontologists and Mineralogists, Tulsa, OK, 1–34.

Doser, D. I. (1990). Source characteristics of earthquakes along the southern San Jacinto and Imperial fault zones (1937 to 1954), *Bull. Seismol. Soc. Am.* **80,** 1099–1117.

Doser, D. I. (1992). Historic earthquakes (1918 to 1923) and an assessment of source parameters along the San Jacinto fault system, *Bull. Seismol. Soc. Am.* **70,** 185–201.

Ellsworth, W. L. (1990). Earthquake history, 1769–1989, in *The San Andreas Fault System, California*, R. E. Wallace (Editor), *U.S. Geol. Surv. Profess. Pap. 1515*, 153–187.

Field, E. H., T. E. Dawson, K. R. Felzer, A. D. Frankel, V. Gupta, T. H. Jordan, T. Parsons, M. D. Petersen, R. S. Stein, R. J. Weldon II, and C. J. Wills (2009). The uniform California earthquake rupture forecast, version 2 (UCERF 2), *Bull. Seismol. Soc. Am.* **99,** no. 4, 2053–2107, doi: 10.1785/0120080049.

Grant, L. B., J. T. Waggoner, T. K. Rockwell, and C. von Stein (1997). Paleoseismicity of the north branch of the Newport–Inglewood fault in Huntington Beach, California, *Bull. Seismol. Soc. Am.* **87,** 277–293.

Harris, R. A., and S. M. Day (1993). Dynamics of fault interaction: Parallel strike-slip faults, *J. Geophys. Res.* **98,** 4461–4472.

Harris, R. A., R. J. Archuleta, and S. M. Day (1991). Fault steps and the dynamic rupture process: 2D numerical simulations of a spontaneously propagating shear fracture, *Geophys. Res. Lett.* **18,** 893–896.

Hempton, M., and K. Neher (1986). Experimental fracture, strain and subsidence patterns over en echelon strike-slip faults: Implications for the structural evolution of pull-apart basins, *J. Struct. Geol.* **8,** 597–605.

Knuepfer, P. L. K. (1989). Implications of the characteristics of end-points of historical surface fault ruptures for the nature of fault segmentation, *U.S. Geol. Surv. Open-File Rept. 89-315*, 193–228.

Lee, T. C., S. Biehler, S. K. Park, and W. J. Stephenson (1996). A seismic refraction and reflection study across the central San Jacinto Basin, southern California, *Geophysics* **61,** 1258–1268.

Lin, G., P. M. Shearer, and E. Hauksson (2007). Applying a three-dimensional velocity model, waveform cross correlation, and cluster analysis to locate southern California seismicity from 1981 to 2005, *J. Geophys. Res.* **112,** no. B12309, doi: 10.1029/2007JB004986.

Mann, P., M. Hempton, D. Bradley, and K. Burke (1983). Development of pull-apart basins, *J. Geol.* **91,** 529–554.

Matti, J. C., D. M. Morton, and B. F. Cox (1985). Distribution and geologic relations of fault systems in the vicinity of the Central Transverse Ranges, southern California, *U.S. Geol. Surv. Open-File Rept. 85-365*.

Matti, J. C., D. M. Morton, and B. F. Cox (1992). The San Andreas fault system in the vicinity of the central Transverse Ranges province, southern California, *U.S. Geol. Surv. Open-File Rept. 92-354*, 40 pp., scale 1:250,000.

Morton, D. M. (1977). Surface deformation in part of the San Jacinto valley, southern California, *J. Res. U.S. Geol. Surv.* **5,** 117–124.

Morton, D. M., and J. C. Matti (1993). Extension and contraction within an evolving divergent strike-slip fault complex: The San Andreas and San Jacinto fault zones at their convergence in southern California, in *The San Andreas Fault System: Displacement, Palinspastic Reconstruction, and Geologic Evolution*, R. E. Powell, R. J. Weldon, and J. C. Matti (Editors), Geol. Soc. Am. Memoir, Vol. 178, 217–230.

Morton, D. M., and J. C. Matti (2001a). Geologic Map of the Lakeview 7.5′ Quadrangle, Riverside County, California, *U.S. Geol. Surv. Open-File Rept. 01-174*, scale 1:24,000, http://geopubs.wr.usgs.gov/open-file/of01-174.

Morton, D. M., and J. C. Matti (2001b). Geologic map of the Sunnymead 7.5′ quadrangle, Riverside County, California, *U.S. Geol. Surv. Open-File Rept. 01-450*.

Naylor, M. A., G. Mandl, and C. H. K. Sijpesteijn (1986). Fault geometries in basement induced wrench faulting under different initial stress states, *J. Struct. Geol.* **8,** 737–752.

Nemser, E. S., and D. S. Cowan (2009). Downdip segmentation of strike-slip fault zones in the brittle crust, *Geology* **37,** no. 5, 419–422, doi: 10.1130/g25619a.1.

Oglesby, D. (2008). Rupture termination and jump on parallel offset faults, *Bull. Seismol. Soc. Am.* **98,** no. 1, 440–447, doi: 10.1785/0120070163.

Onderdonk, N. W., T. K. Rockwell, S. F. McGill, and G. I. Marliyani (2013). Evidence for seven surface ruptures in the past 1600 years on the Claremont fault at Mystic Lake, northern San Jacinto fault zone, California, *Bull. Seismol. Soc. Am.* **103,** no. 1, 519–541, doi: 10.1785/0120120060.

Park, S., D. Pendergraft, W. Stephenson, K. Shedlock, and T. Lee (1995). Delineation of intrabasin structure in a dilational jog of the San Jacinto fault zone, southern California, *J. Geophys. Res.* **100,** no. B1, 691–702.

Rahe, B., D. A. Ferrill, and A. P. Morris (1998). Physical analog modeling of pull-apart basin evolution, *Tectonophysics* **285,** 21–40, doi: 10.1016/S0040-1951(97)00193-5.

Rasmussen, G. S. (1981). Nature of surface rupture and recurrence interval, Casa Loma fault, in *Geology of the San Jacinto Mountains: South Coast Geological Society*, A. R. Brown and R. W. Ruff (Editors), Annual Field Trip Guidebook, Vol. 9, 48–54.

Rockwell, T. K., J. A. Dewhurst, C. W. Walls, W. J. Pollard, A. Orgil, G. Faneros, and T. E. Dawson (2000). High-resolution paleoseismology in southern California: Investigation of segment controls on the rupture history of the southern San Jacinto fault, in *Active Fault Research for the New Millenium, Proceedings of the Hokudan International Symposium and School on Active Faulting*, K. Okumura, K. Takada, and H. Goto (Editors), *Letter Press Ltd.*, Hiroshima, Japan, 413–419.

Rockwell, T. K., G. Seitz, T. Dawson, and J. Young (2006). The long record of San Jacinto fault paleoearthquakes at Hog Lake: Implications for

regional patterns of strain release in the southern San Andreas fault system, *Seismol. Res. Lett.* **77,** 270.

Rodgers, D. A. (1980). Analysis of pull-apart basin development produced by en echelon strike-slip faults, in *Sedimentation in Oblique-Slip Mobile Zones*, P. F. Ballance and H. G. Reading (Editors), Special Publication International Association of Sedimentologists, 4, 27–41.

Salisbury, J. B., T. K. Rockwell, T. J. Middleton, and K. W. Hudnut (2012). LiDAR and field observations of slip distribution for the most recent surface ruptures along the Central San Jacinto fault, *Bull. Seismol. Soc. Am.* **102,** 598–619.

Sanders, C. O., and H. Kanamori (1984). A seismotectonic analysis of the Anza Seismic Gap, San Jacinto fault zone, Southern California, *J. Geophys. Res.* **89,** 5873–5890.

Sanders, C., and H. Magistrale (1997). Segmentation of the northern San Jacinto fault zone, southern California, *J. Geophys. Res.* **102,** 27,453–27,467.

Sanders, C. O., H. Magistrale, and H. Kanamori (1986). Rupture patterns and preshocks of large earthquakes in the southern San Jacinto fault zone, *Bull. Seismol. Soc. Am.* **76,** 1187–1206.

Segall, P., and D. D. Pollard (1980). Mechanics of discontinuous faults, *J. Geophys. Res.* **85,** 4337–4350.

Sharp, R. V. (1967). San Jacinto fault zone in the Peninsular ranges of southern California, *Geol. Soc. Am. Bull.* **78,** 705–730.

Sharp, R. V. (1972). Map showing recently active breaks along the San Jacinto fault zone between the San Bernardino area and Borrego Valley, California, scale 1:24,000, *U.S. Geol. Surv. Misc. Geologic Investigations Map, I-675*.

Sharp, R. V. (1975). En echelon patterns of the San Jacinto Fault Zone, *Special Report California Division of Mines Geology* **118,** 147–152.

Sibson, R. H. (1986). Rupture interaction with fault jogs, in *Earthquake Source Mechanics*, S. Das, J. Boatwright, and C. H. Scholz (Editors), American Geophysical Monograph, **37**, 157–167.

Tchalenko, J. (1970). Similarities between shear zones of different magnitudes, *Geol. Soc. Am. Bull.* **81,** 1625–1640.

Thatcher, W., J. A. Hileman, and T. C. Hanks (1975). Seismic slip distribution along the San Jacinto fault zone, southern California, and its implications, *Geol. Soc. Am. Bull.* **86,** 1140–1146.

Toppozada, T. R., C. B. Real, and D. L. Parke (1981). Preparation of isoseismal maps and summaries of reported effects for pre-1900 California earthquakes, *Calif. Div. Mines and Geol. Open-File Rept. 81-11*, SAC.

Wallace, R. E. (1990). Geomorphic expression, in *The San Andreas Fault System, California*, R. E. Wallace (Editor), *U.S. Geol. Surv. Profess. Pap. 1515*, 14–58.

Wesnousky, S. G. (1986). Earthquakes, Quatemary faults, and seismic hazard in California, *J. Geophys. Res.* **91,** 12,587–12,631.

Wesnousky, S. (1994). The Gutenberg–Richter or characteristic earthquake distribution, Which is it? *Bull. Seismol. Soc. Am.* **84,** no. 6, 1940–1959.

Wesnousky, S. (2006). Predicting the endpoints of earthquake ruptures, *Nature* **444,** 358–360.

Working Group on California Earthquake Probabilities (WGCEP) (1995). Seismic hazards in southern California: Probable earthquakes, 1994–2024, *Bull. Seismol. Soc. Am.* **85,** 379–439.

Working Group on California Earthquake Probabilities (WGCEP) (2007). The Uniform California Earthquake Rupture Forecast, Version 2 (UCERF 2), *U.S. Geol. Surv. Open-File Rept. 2007-1437*, and *California Geol. Surv. Special Rept. 203*.

Zachariasen, J., and K. Sieh (1995). The transfer of slip between two en echelon strike-slip faults: A case study from the 1992 Landers earthquake, southern California, *J. Geophys. Res.* **100,** 15,281–15,302.

Department of Geological Sciences
San Diego State University
5500 Campanile Drive
San Diego, California 92182
gayatri.marliyani@asu.edu
trockwell@geology.sdsu.edu
(G.I.M., T.K.R.)

Department of Geological Sciences
California State University Long Beach
1250 Bellflower Boulevard
Long Beach, California 90840-3902
nate.onderdonk@csulb.edu
(N.W.O.)

Department of Geological Sciences
California State University, San Bernardino
5500 University Parkway
San Bernardino, California 92407-2318
smcgill@csusb.edu
(S.F.M.)

Manuscript received 14 July 2012